High-energy phonon pulses in liquid ^{4}He

Ruslan V. Vovk, Charles D. H. Williams, and Adrian F. G. Wyatt
School of Physics, University of Exeter, Exeter, EX4 4QL, United Kingdom
(Received 5 December 2003; published 30 April 2004)

We have discovered a method for selectively detecting high-energy phonons which has enabled us to make detailed measurements of the shapes of high-energy phonon pulses in liquid ^{4}He at $\approx$50 mK. These phonons are created from pulses of low-energy phonons, injected into the helium by a heater. We suppress the detection of the low-energy phonons by orienting a thin film superconducting Zn bolometer at an angle to the phonon beam. We find that the high-energy phonons are created continuously along the propagation path. As there is also velocity dispersion, the signal at any time is due to a range of phonon energies. Computer simulations of the signals from short pulses reproduce the main features of the measured results. The behavior of the high-energy phonon signals as functions of heater power and pulse length are analyzed and this leads us to suggest how the low-energy phonon pulse develops. In the following paper [I. N. Adamenko *et al.*, Phys. Rev. B **69**, 144525 (2004)] the pulse shape for short pulses is derived analytically.

DOI: 10.1103/PhysRevB.69.144524 PACS number(s): 67.40.−w, 67.90.+z

I. INTRODUCTION

That low-energy phonons, *l*-phonons, can convert to high-energy phonons, *h*-phonons, is an unexpected and remarkable consequence of phonon anisotropy in liquid ^{4}He. The liquid itself is isotropic, but a phonon system can be created within it which is highly anisotropic. The phonon scattering which creates the *h*-phonons depends on the angle between the interacting phonons, and the anisotropic distribution of phonons can favor energy up-scattering over down-scattering. The pulse of *h*-phonons, created from a pulse of *l*-phonons, has a characteristic shape which contains information on the intricate formation process. In this paper we describe a discovery that has enabled us to detect the *h*-phonons separately from the *l*-phonons. We present an extensive set of measurements of *h*-phonon pulses, at different heater powers and pulse lengths, and analyze their behavior. We are led to a surprising conjecture about the development of the *l*-phonon pulse as it propagates.

Experiments show that a short pulse of *l*-phonons can create *h*-phonons which follow behind the *l*-phonon pulse as it propagates.[2] These *h*-phonons have essentially infinite lifetime if there are no thermal phonons. Thus the detected signal from a heater pulse shows two components, with the peaks of the *l*- and *h*-phonons well separated in time as shown in Fig. 1(b). The behavior of anisotropic phonon systems in liquid ^{4}He has been measured and modeled in the last few years with some progress in understanding the subtleties involved.[3–5]

The heater pulse creates a thin sheet of low-energy phonons in the liquid ^{4}He. The area of the sheet is initially the same as the area of the heater, 1×1 mm^2 and its thickness is ct_p, where c is the sound velocity and t_p is the duration of the heating pulse. This sheet propagates in a direction normal to the heater with velocity c. The *l*-phonons interact strongly by three phonon processes 3pp (Refs. 6,7) within the sheet and come into equilibrium with a Bose-Einstein distribution at a temperature T. The liquid ^{4}He can be considered to be at zero temperature and the ambient phonons can be neglected. The anisotropic feature of this phonon system is that only a narrow cone in momentum space is occupied. The small cone angle is a consequence of the small angles allowed by the energy and momentum conservation in 3pp scattering. The cone half angle θ is $\geqslant\theta_{3pp}$, where θ_{3pp} is typically 10°.[4]

The well-defined range of phonon energies that can spontaneously decay, $0<\epsilon<10$ K is a consequence of the shape of the dispersion curve at zero pressure.[8–10] The small deviation of $\omega(q)$ above $\omega=cq$ in this energy range allows rapid spontaneous decay as energy and momentum can be conserved.[11,12] At $\epsilon>10$ K, the deviation is below $\omega=cq$ and spontaneous decay is forbidden and essentially only four phonon processes 4pp are allowed. The *h*-phonons are defined as those phonons with energy $\geqslant$10 K. The initial upward deviation of $\omega(q)$ from linearity is slight but it has considerable consequences.

The *h*-phonons are created from the energetic tail of the *l*-phonon spectrum through 4pp.[13–16] The created *h*-phonons have a substantially lower group velocity, $\leqslant$189 m s^{-1}, than the *l*-phonon pulse, 238 m s^{-1}. This means that the *h*-phonons rapidly fall behind the *l*-phonon pulse and then propagate as independent wave packets behind the *l*-phonons. There can be 4pp interactions between these *h*-phonons[5] but usually their density is so low that they can be ignored.

The *h*-phonons are created continuously as the *l*-phonon sheet moves away from the heater and they can be created more than 5 mm from the heater.[17] The group velocity of phonons with $\epsilon\geqslant10$ K decreases with phonon energy, so the *h*-phonons disperse. Hence the signal at a particular time will be due to a range of phonon energies from phonons created at different positions and times in the liquid ^{4}He.

We would like to know the spectrum of *h*-phonons that is created as this is important for other experiments which use these *h*-phonons, for example, quantum evaporation. We proceed in two stages. The first is to find the pure *h*-phonon signal, which is free from any *l*-phonon signal. The second stage is to simulate the *h*-phonon signal, putting in as much physics as we can. The simulated signal is similar to the measured one and this gives some confidence that the simu-

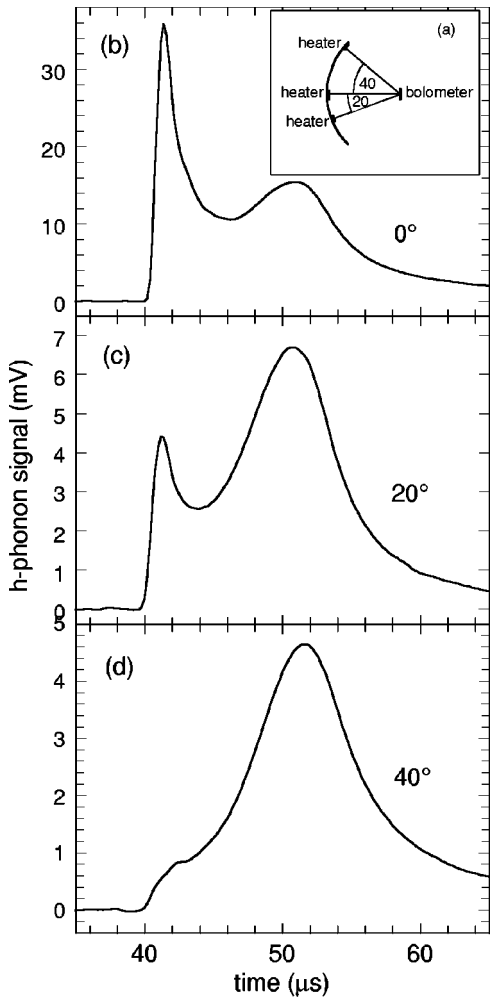

FIG. 1. The experimental arrangement is shown schematically in (a). Typical signals are shown in (b), (c), and (d), as function of time, measured from the start of the heater pulse, for the angles of incidence on the bolometer of 0°, 20°, and 40°, respectively. The first peak is due to the *l*-phonons and the second due to the *h*-phonons. The heater pulses are 12.5 mW and 100 ns. Note how the *l*-phonon signal decreases with angle, (d) is almost entirely due to *h*-phonons.

lation is a correct representation of short pulse behavior. The spectrum of phonons can then be readily obtained from the simulation. The simulation has been treated computationally in this paper and analytically in the succeeding paper,[1] and the results are in agreement.

In Sec. II we describe the experiment and in Sec. III we present *h*-phonon pulse shapes at different heater pulse lengths and powers. In Sec. IV we analyze the pulse shapes and discuss them. This exposes the areas where more research is required. In Sec. V we describe the model and compare its simulated pulse shapes with the measured ones at low power and pulse length. Finally, we draw conclusions in Sec. VI.

II. THE EXPERIMENT

In this experiment six heaters are arranged in an arc and all face a bolometer which is at the center of the arc, 9.53 mm from each heater, see Fig. 1(a). The heaters are thin gold films 1×1 mm^2 with resistance $\sim50\ \Omega$, evaporated onto glass cover slips 1×6 mm^2. These are glued onto a carefully machined brass piece, which is part of a cylinder of radius 10 mm, with thin GE varnish. The bolometer is a zinc film, 1×1 mm^2, cut into a serpentine track with resistance at room temperature $\sim300\ \Omega$. At low temperatures this is held at $\sim50\ \Omega$, on the superconducting transition edge, by a feedback circuit.[18] The superconducting transition temperature is lowered to ~350 mK with a constant external magnetic field. The feedback current to the bolometer is proportional to the power absorbed. The signal is amplified by a broad band, DC–1 MHz, amplifier (EG&G 5113) and then recorded with a Tektronix DSA 601A. Many repetitions are averaged to improve the signal to noise ratio. The responsivity of the detection system is 6.03×10^3 V/W.

Current pulses are applied to the heater in the range 30–350 ns from a pulse generator (LeCroy 9210) creating heater powers in the range 3–25 mW. The pulse generator has a minimum rise and fall time of 5 ns each and this was always used. This means that the energy-averaged pulse length is ≈7 ns shorter than the nominal values which are always quoted in this paper. This clearly has more effect on short pulses than long ones.

The experimental cell is cooled by a dilution refrigerator to ~50 mK. The cell is filled with isotopically pure ^{4}He (Ref. 19).

Typical signals are shown in Figs. 1(b), 1(c), and 1(d) from heaters at angles 0°, 20°, and 40°, see Fig. 1. At 0° the propagation path is perpendicular to the bolometer and the usual signal shape is obtained, see Fig. 1(b). The *l*-phonons give a narrow peak starting at 40 μs and the *h*-phonons give the broad peak with maximum at ~51 μs. At 20° both *l*- and *h*-phonon signals are smaller than at 0°, but the *l*-phonon signal has decreased more, see Fig. 1(c). This is solely due to the propagation being at 20° to the bolometer normal. When this angle is 40°, we see in Fig. 1(d), that the *l*-phonons are hardly detected while the *h*-phonon signal is clear. We used this heater at 40° to take all the results presented in this paper. Using this technique we have obtained the *h*-phonon signals which are almost free of *l*-phonons and the problem of trying to separate the *l*- and *h*-phonon signals, as for example in Fig. 1(b), is circumvented.

We now discuss the reason why the *l*-phonons are not detected at oblique angles. The *l*-phonons have low energy and long wavelength and act like classical waves. In classical acoustic theory,[20] frequency and the parallel component of wave vector are conserved on transmission through a plane interface between two materials. There is then a critical angle, on the low velocity side of the interface given by $\sin^{-1}(v_1/v_2)$, where v_1 and v_2 are the velocities of sound in the two materials. This angle is very small for the interface between liquid helium and most solids, so there is a critical cone for transmission on the helium side of the boundary.[21] Very low-energy phonons, outside of this critical cone, do not give any energy to the solid detector.

However for higher energy phonons, there are two channels for transmission, the classical one and another one in

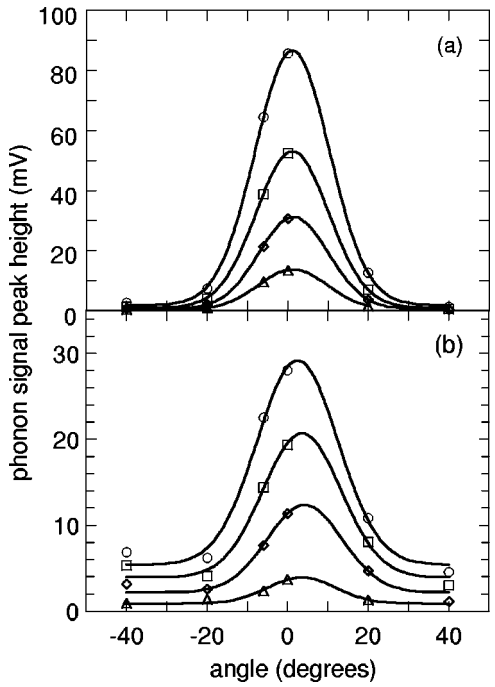

FIG. 2. The *l*- and *h*-phonon peak heights are shown in (a) and (b), respectively, as functions of angle of incidence on the bolometer, for different power heater pulses. Circles, 25 mW; squares, 12.5 mW; diamonds, 6.3 mW; and triangles, 3.2 mW. The pulse duration is 150 ns. Note that the *l*-phonon peak height is essentially zero at 40°. The lines are guides for the eye.

which parallel momentum[22] and energy[23] are not conserved. This has been termed the background channel.[22] Whereas the transmission via the classical channel is weak and independent of energy, this is not so for the background channel. From experiment,[24,25] we know that the transmission coefficient for this channel rises linearly for phonons with energy $0<\epsilon<5$ K and then is constant for $\epsilon>5$ K. It is the background channel, which gives rise to the anomalously high interface conductance known as the Kapitza conductance.[24] So, high-energy phonons incident at angles outside the classical critical cone, can transmit some energy into the detector via the background channel. For *h*-phonons with energy $\epsilon \geqslant 10$ K, the transmission is independent of phonon energy.[25] The *l*-phonon angular dependence will not show an abrupt cutoff at the critical angle if the surface of the detector is not perfectly flat, also there will be some small transmission via the background channel for *l*-phonons at $T=0.7$ K with typical energy $\epsilon \sim 1.1$ K.

In Figs. 2(a) and 2(b) we show the peak heights of the *l*- and *h*-phonons signals, respectively, as a function of angle. The *l*-phonons' peak heights follow a Gaussian shape centered at zero with a half-width at half maximum (hwhm) of 11° and 10° for the 25 mW and 6.3 mW data, respectively, and the peak height is essentially zero at $\pm 40°$. The *h*-phonons' peak heights do not fall to zero, as the *l*-phonons do, but fall to what appears to be constant values by $\pm 40°$. If these values are treated as base lines, the data points also follow Gaussian shapes with similar hwhms. It is the fact that the *h*-phonon signals do not fall to zero at $\pm 40°$ that enables us to study the *h*-phonons with negligible contribution from the *l*-phonons.

The angular width of the Gaussians is approximately twice that of the critical angles for classical acoustic transmission from liquid helium to solid Zn, 5.6°. This is to be expected if the angular cutoff is due to incident phonons being outside of the critical cone for a Zn surface that is not flat. These data imply that the normal to the crystallites, making up the surface of the Zn, have a distribution with half-width approximately $\pm 5°$ to the surface normal. This small angular range is also consistent with the fact that it was difficult to detect any surface structure of the Zn with a scanning electron microscope for this bolometer.

III. *h*-PHONON PULSE SHAPES

In Figs. 3(a)–3(d) we present the measured *h*-phonon pulses for the heater at 40°, for the heater power 3.2, 6.3, 12.5, and 25 mW. The figures show the results for pulse lengths in the range 30–350 ns. We briefly describe how this signal is formed to give a context for the discussion. More details are given in Sec. V on the modeling.

The *l*-phonons propagate at the sound velocity *c* and it takes 40 μs to travel the distance $l=9.53$ mm to the bolometer. At every position the *l*-phonon pulse creates a spectrum of *h*-phonons with $\epsilon \geqslant 10$ K. The spectrum decreases monotonically from the peak at $\epsilon=10$ K. These *h*-phonons are lost from the back of the *l*-phonon pulse and travel at their momentum-dependent group velocity $v_g(p)$ to the bolometer. The *h*-phonons created just in front of the bolometer, arrive at the same time as the *l*-phonons, and those created near the heater arrive at a later time given by $l/v_g(p)$. Thus phonons with $\epsilon=10$ K arrive between 40 and 50.4 μs and higher energy ones arrive in a longer time interval.

The signal peaks at ≈ 50 μs because it is dominated by $\epsilon=10$ K phonons created near the heater where the *l*-phonon pulse is hottest. This is due to the creation rates increasing strongly with temperature[5] and the fact that the *l*-phonon pulse cools as it moves away from the heater; it loses energy by emitting *h*-phonons. Further from the heater the creation rate is lower and so the earlier arriving signal is smaller. The signal arriving later than ≈ 50.4 μs decreases with time because it is due to higher energy *h*-phonons whose creation rate decreases with energy.[5]

The *l*-phonon pulse is considered to be short if the *h*-phonons leave it without being scattered by *l*- or *h*-phonons. Then only the creation rate is important. The condition that the pulse is short is[4]

$$t_p \ll \frac{c-v_g}{c\nu_{\rm eff}} \tag{1}$$

where $\nu_{\rm eff}$, the effective decay rate, is given by,[26,27]

$$\nu_{\rm eff}=[\nu_d^{(1)2}+4\overline{\nu}_{b1}\nu_d^{(2)}]^{1/2} \tag{2}$$

and $\nu_d^{(1)}=\overline{\nu}_{d1}+\overline{\nu}_{d3}-\overline{\nu}_{b4}\approx\overline{\nu}_{d1}$ and $\nu_d^{(2)}=\overline{\nu}_{d4}-\overline{\nu}_{b3}\approx\overline{\nu}_{d4}/2$, where subscripts b and d refer to creation and annihilation processes, respectively, the subscripts 1, 3, and 4 indicate the different types of 4pp scattering defined in Refs. 26 and 27,

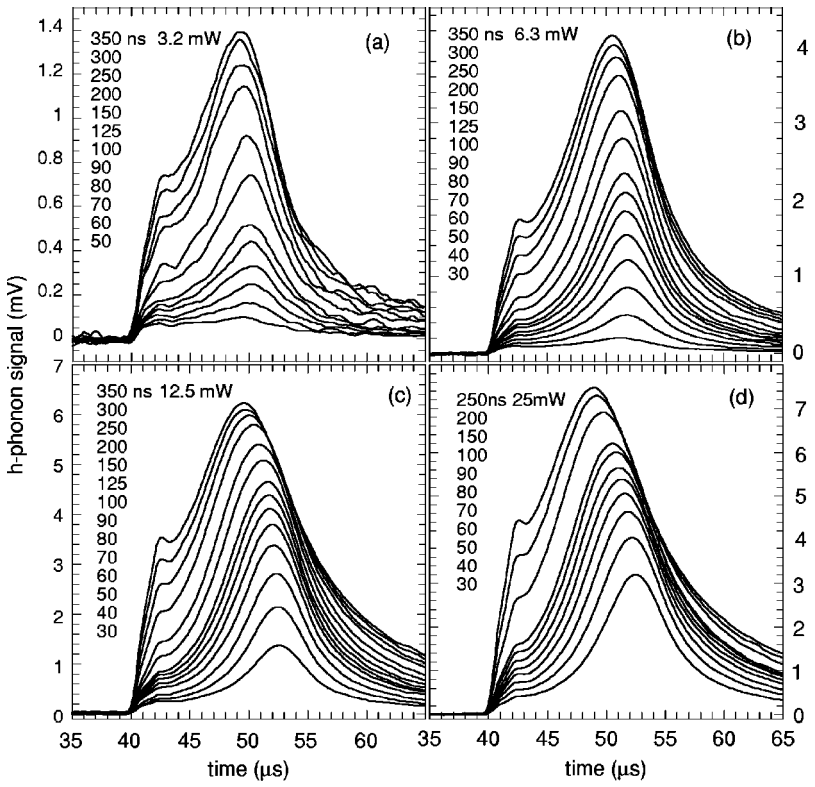

FIG. 3. The measured signals at 40° as function of time from the heater pulse, for different pulse lengths. The heater powers are 3.2 mW, 6.3 mW, 12.5 mW, and 25 mW in (a), (b), (c), and (d), respectively. The signals are essentially due to the *h*-phonons with a small contribution from the *l*-phonons around 42 μs.

and the bar indicates an average over the *h*-phonon momentum vectors.[26,27] Using the values in Fig. 3 of Ref. 28, we find that t_p must be much less than 360 ns, 810 ns, and 2 μs for $T_i=1$ K, 0.9 K, and 0.8 K, respectively, i.e., for short pulses $t_p \leqslant 36$ ns, 81 ns, and 200 ns, respectively. The peak in the *h*-phonon spectrum is at $\epsilon=10$ K and for these phonons the decay rates are higher so the pulse length has to be shorter than for average *h*-phonons, e.g., at $T_i=1$ K, $t_p \ll 120$ ns for 10 K phonons, which is one third of the average value.

If the *l*-phonon pulses are long, then the 4pp scattering within the pulse and possibly amongst the following *h*-phonons, cannot be ignored. The effects of this scattering will be to delay the emission of *h*-phonons, change the energy spectrum of *h*-phonons and create a suprathermal distribution.[4,28] This latter effect will also increase the scattering rates. With all these ideas in mind we return to the *h*-phonon pulse shapes.

A number of features can be immediately seen in Fig. 3. The *h*-phonon signals all start at the same time which is also the time of the start of the *l*-phonons. This signal is due to *h*-phonons that are created just in front of the bolometer, from *l*-phonons that have traveled at velocity *c*. Some vestige of the *l*-phonon signal can be seen in the early part of the signals. At 40°, we estimate that the *l*-phonon signal contributes less than 5% at 42.5 μs and $<1\%$ at $\geqslant 43.5$ μs. The *h*-phonon signal rises steeply at 40 μs for 2 μs and then almost levels off. Then the rise increases and the *h*-phonons reach a peak at ≈ 50 μs. The position of the peak shifts to lower times with increasing pulse length and power.

After the peak, the *h*-phonon signal smoothly and rapidly decreases with time. However, there is a substantial signal at long times, $\geqslant 60$ μs. This would seem to indicate that higher energy *h*-phonons are created with lower group velocities. However, this very-late arriving signal is probably due to an artifact caused by some of the incident energy being stored in the bolometer substrate and then leaking out slowly. We ignore these signals until their origin has been clarified. However, the shapes of the graphs involving integrals, which we show later, are not qualitatively changed if the integrals have an upper limit of 80 μs rather than 60 μs.

We now examine the times of the peak in detail. For 3.2 mW, the time of the peaks changes least. It goes from 49.5 μs at $t_p=50$ ns to 50.5 μs at 80 ns, and 49.8 μs at 200 ns. For 6.3 mW the peak times are: 51.9 μs at 50 ns and monotonically decreases to 51.2 μs at 200 ns. For 12.5 mW the peak times change more: 52.3 μs at 50 ns to 50.4 μs at 200 ns. For 25 mW the change is largest: 52.0 μs at 50 ns to 49.2 μs at 200 ns. The time of arrival of 10 K phonons created near the heater is $40\times 238.3/189=50.4$ μs, so the faster times of arrival of the peak, at high pulse powers, suggests that the main creation of *h*-phonons takes place some distance in front of the heater, as phonons that are created later, arrive earlier. For the peak at 49.2 μs, this distance is 1.1 mm. We think this is probably due to the time it takes for the *h*-phonon population in a long pulse to buildup to a dynamic equilibrium. The finite time constant t_c, of the detection system delays the peak by approximately 0.5 t_c. Then for $t_c=1.5$ μs the peak would be at 48.4 μs if there were no time constant and this would change the value above to 1.8 mm.

In Fig. 4 we show the peak height as a function of pulse length for four pulse powers. We immediately see that the peak height does not increase linearly with pulse length. In-

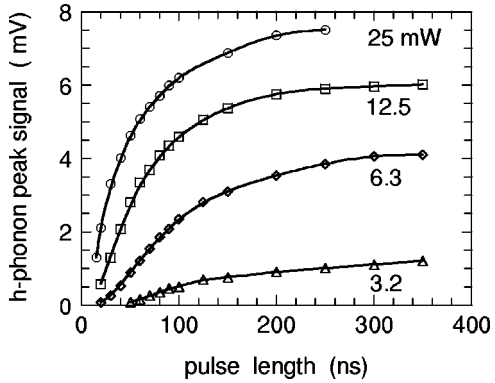

FIG. 4. The *h*-phonon peak height is shown as a function of heater pulse length, at different heater powers. The curves are linear initially and at longer pulse lengths approach saturation. The linear sections extrapolate to nonzero pulse length due to the rise and fall time of the heater pulse and the time for the heater to reach a dynamic equilibrium temperature.

stead it shows an initial linear increase (except at very short pulse lengths, $t_p < 30$ ns, where the rise and fall times of the pulse are significant, as is also the time for the heater to reach an equilibrium temperature) and then a turnover towards saturation. The linear increase, reported in Ref. 1 for short pulses, ends at 100 ± 20 ns at 3.2 mW, 80 ± 10 ns at 6.3 mW, 50 ± 5 ns at 12.5 mW, and 20 ± 5 ns at 25 mW. We also see that the nearly saturated values of the peak heights do not scale with pulse power. We conclude from Fig. 4, that the short-pulse behavior, where the response is linearly dependent on pulse length, is confined to the lowest powers and pulse lengths.

Figure 5 shows the peak height as a function of pulse energy ($t_p \times$ pulse power). We see that the data partially collapse onto a universal curve, which shows an initial linear increase with a subsequent turnover towards saturation. The curves at different powers, peel-off from the universal line at points which increase with pulse power. This indicates that the peak height is increased when a given pulse energy is contained in a shorter pulse. This is to be expected, because for a given energy, the pulse temperature increases as the pulse length decreases, and the creation rate of *h*-phonons

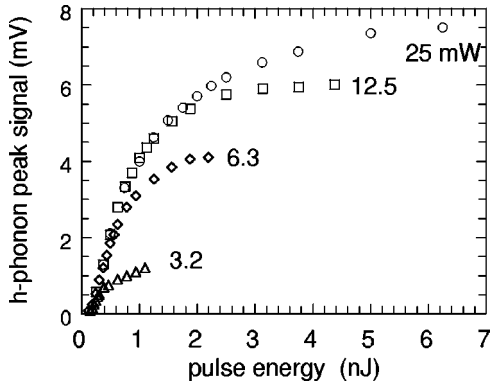

FIG. 5. The *h*-phonon peak height is shown as a function of heater pulse energy for different powers. It can be seen that the data for shorter pulses collapse onto a universal curve.

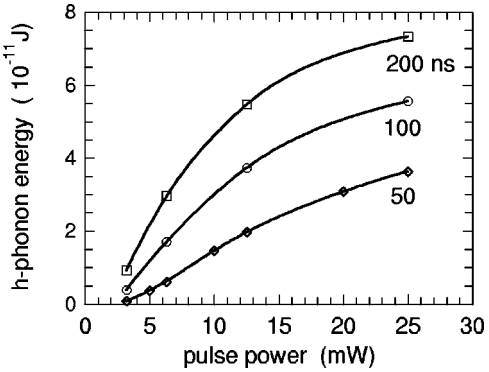

FIG. 6. The *h*-phonon signal, integrated from 40 μs to 60 μs, is shown as a function of heater power for three different pulse lengths 50 ns, 100 ns, and 200 ns. Note that the curve is most nearly linear at the shortest pulse length.

from *l*-phonons increases with temperature as $\nu_{b1} \propto \exp(-3.18\ [\mathrm{K}]/T)$, see Eq. (8) and Ref. 1. The saturation at long pulse lengths is due to the *h*-phonon population increasing to a dynamic equilibrium within the *l*-phonon pulse. It will be a suprathermal distribution, determined by the temperature-dependent creation and decay rates.[4,26–28]

IV. CHARACTERISTICS OF THE *h*-PHONONS

In this section we consider the integrated *h*-phonon energy. As the phonon transmission coefficient from helium to the solid Zn is independent of phonon energy above $\epsilon > 5$ K, the integral of the received signals over time is proportional to the energy. In Fig. 6 we show the integral of the *h*-phonon signal from 40 to 60 μs as a function of power for pulse lengths of 50, 100, and 200 ns. We see that total energy in the *h*-phonons increases with pulse power, initially linearly and then more slowly. At shorter pulse lengths, the linear region is longer. In the linear region, approximately the same fraction of the heater energy finally appears as *h*-phonons.

The energy density E_l of the *l*-phonons pulse is given by

$$E_l = \frac{\Omega_p \pi k^4 T^4}{120 \hbar^3 c^3}, \tag{3}$$

where Ω_p is the occupied solid angle in momentum space. We have previously shown that E_l is proportional to the heater pulse power W,[29] so that $\Omega_p T^4 \propto W$. We propose that both Ω_p and T vary with W but it is the variation of Ω_p that is more important at high powers, and the variation of T with W, mainly occurs at low powers, $W < \sim 7$ mW. This is suggested by the ratio of the peak height to the signal at 43.5 μs for 50 ns pulses at different powers. The values of this ratio are 0.61, 0.20, 0.14, and 0.17 for 3.2 mW, 6.3 mW, 12.5 mW, and 25 mW, respectively. From the model in Sec. V (which neglects interactions between the *h*-phonons which may be important at higher powers), we find values of this ratio for different T_l are: 0.54, 0.37, 0.17, and 0.11 for $T_l = 0.75$ K, 0.8 K, 0.9 K, and 1 K, respectively. This suggests that the measured values of the ratios correspond to $T_l < \sim 0.9$ K and

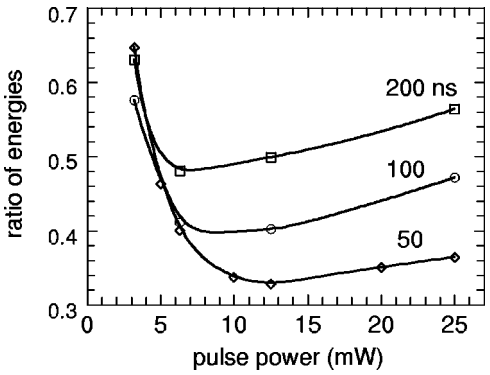

FIG. 7. The ratio of the *h*-phonon signal, integrated from 40 μs to 50.4 μs, to that integrated from 40 μs to 60 μs, as a function of the pulse power, for pulse lengths 50 ns, 100 ns, and 200 ns. Note the rapid decrease in the early-arriving signal ($t<50.4$ μs) at low powers for all the pulse lengths.

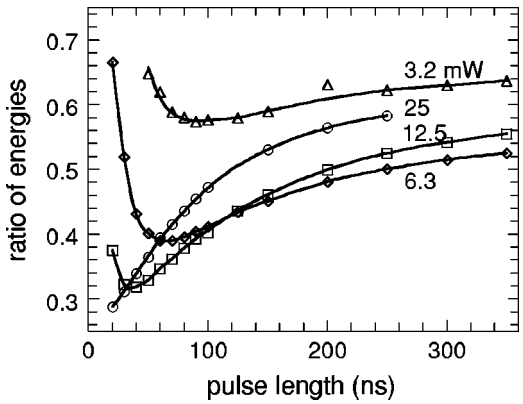

FIG. 8. The ratio of the *h*-phonon signal, integrated from 40 μs to 50.4 μs, to that integrated from 40 μs to 60 μs, as a function of the pulse length, for heater powers of 3.2, 6.3, 12.5, and 25 mW. Note the decrease with pulse length ends at shorter pulse lengths as the heater power is increased.

this temperature is reached around 7 mW. The measured ratio is approximately constant above this power which implies that the initial temperature is then reasonably constant at $\sim$0.9 K, and the energy density then increases with power due to Ω_p increasing. From $\sim$6.3 mW to 25 mW, $\Omega_p \propto W$, so Ω_p increases by a factor $\sim$4. As $\Omega_p = 2\pi(1-\cos\theta) = \pi\theta^2$ for small angles, we see that the cone angle only increases by a factor of $\sim$2. If $\theta \sim 10°$ at $\sim$6.3 mW, then $\theta = \sim 20°$ at 25 mW, which can still be considered a small cone. It is not yet clear what process causes Ω_p to increase with power.

The initial linear relationship between the energy in the *h*-phonons and the pulse power shown in Fig. 6, we suggest arises as follows. For power above $\sim$7 mW, the energy density in the *l*-phonon sheet is due to Ω_p increasing at constant temperature, $T_l \sim 0.9$ K. The rate of creation of *h*-phonons is then only proportional to the density of *l*-phonons, which is proportional to Ω_p and hence the pulse power. For power $<\sim$7 mW, T_l decreases with power and the creation rate of *h*-phonons falls faster than the decrease in power because the rate decreases with temperature. The relationship between energy in the *h*-phonons and pulse power in this range will depend on the propagation distance.[4] The longer the distance, the greater the fraction of *l*-phonon energy is converted to *h*-phonons. In this range we should expect the relationship to fall below linear.

In Fig. 7 we show the ratio of the signal integrated from 40 μs to 50.4 μs to that integrated from 40 μs to 60 μs. This gives a measure of the number of *h*-phonons near $\epsilon = 10$ K relative to the total number of *h*-phonons. The ratio is plotted as a function of pulse power for pulse lengths of 50, 100, and 200 ns. We see that at low power, the ratio decreases rapidly with power. This behavior can be understood as follows. At the lowest pulse power, most of the *h*-phonons are created with energy near $\epsilon = 10$ K. As the power is increased, the proportion of higher energy phonons increases and as these have lower group velocities, they contribute more outside the time window from 40 μs to 50.4 μs. This behavior suggests that *h*-phonons can be created with energies significantly greater than 10 K.

The same ratio plotted in Fig. 7 is shown against pulse length in Fig. 8. At low power, there is only a small variation, with pulse length, of the fraction of energy arriving before 50.4 μs. This can be seen directly in Fig. 3 where the pulse shape changes little with pulse length. However, for higher pulse powers, the change is considerable. For short pulses, the fraction of energy before 50.4 μs decreases rapidly with the pulse length. This behavior is not seen at 25 mW, presumably because it occurs at shorter pulse lengths than were measured. The decrease is most clearly seen at 6.3 mW and can be seen at 12.5 mW and 3.2 mW. The maximum pulse length for this behavior is a strong function of power: it is less than 20 ns at 25 mW, and is 38 ns at 12.5 mW, 68 ns at 6.3 mW, and 90 ns at 3.2 mW.

The explanation given for the behavior in Fig. 7 also applies to Fig. 8. For short pulse lengths, an increasing number of high energy and low velocity phonons are created as the pulse length is increased. At longer pulse lengths the fraction of energy arriving before 50.4 μs increases for all powers. This is most likely due to the *h*-phonons being trapped in the *l*-phonon pulse for longer periods. The *h*-phonons are then emitted further from the heater and so arrive earlier, as they have traveled further at the higher velocity. In other words, long pulses cool more slowly than short pulses, and so emit *h*-phonons nearer to the detector.

In Figs. 9(a) and 9(b) we show the integral of the *h*-phonon signal over two ranges 40–50.4 μs and 40–60 μs, against pulse energy. We see universal curves similar to that shown in Fig. 5 for the peak height. The early arriving *h*-phonons, 40–50.4 μs, show a long linear region and only a small deviation from linearity at high pulse energies. The signal integrated over 40–60 μs shows a shorter linear region and then a considerable deviation from linearity. As the early signal, 40–50.4 μs, is mainly due to *h*-phonons near 10 K, we see that the number of these phonons is nearly proportional to the pulse energy. This suggests that these *h*-phonons are emitted by the *l*-phonon pulse without any scattering within the pulse. The *h*-phonons with $\epsilon = 10$ K that are scattered to other *h*-phonons must create higher energy phonons, because $\epsilon = 10$ K is the minimum energy. Higher

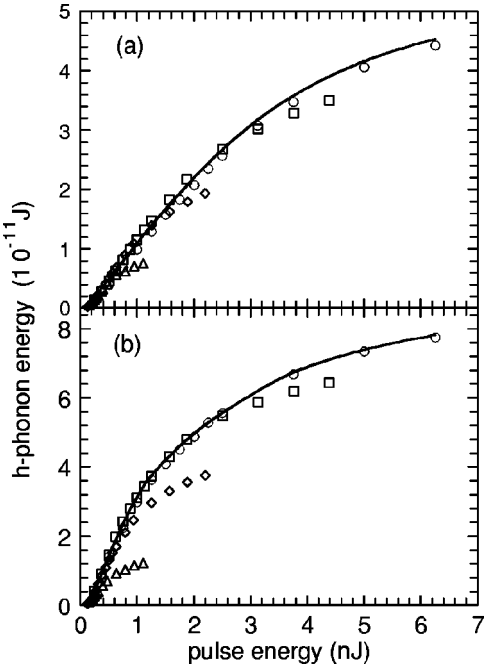

FIG. 9. The *h*-phonon signal integrated from 40 μs to 60 μs in (a) and from 40 μs to 50.4 μs in (b) as a function of pulse energy. Note the collapse of the shorter pulse length data onto universal curves, which are linear at low energies but tend to saturation at high energies. The early arriving signal 40–50.5 μs falls on the universal curve for longer pulse lengths than the total signal represented by the integral over 40–60 μs.

energy phonons contribute more to the signal later than 50.4 μs as they have lower group velocities. However, these phonons are not emitted at such a high rate as the $\epsilon = 10$ K phonons and so the integrated signal over 40–60 μs shows a tendency to saturate at high pulse energies. The theory of the phonon spectrum in a long pulse and the subsequent emission of *h*-phonons has yet to be developed.

In summary, we suggest that there is a limit to the highest temperature of the *l*-phonons. It appears to be around 0.9 K at around 7 mW pulse power. At higher powers the energy in the *l*-phonons increases by the occupied solid angle in momentum space increasing. The results at higher powers and longer pulse lengths indicate that the creation of phonons with energies substantially higher than $\epsilon = 10$ K is important. The high scattering rate of *h*-phonons within the pulse by 4pp, of type b2 (Ref. 5), is the likely cause.

V. THE MODEL

We have modeled the creation of *h*-phonons in a computer simulation. It only treats short pulses which means that once a *h*-phonon has been created within the *l*-phonon pulse, it is lost from the back of the pulse and then is completely stable and noninteracting. The *l*-phonon pulse can in principle cool by *h*-phonon emission and by lateral expansion. However, the modeling showed that cooling by geometric expansion[27] caused the *h*-phonon creation to be concentrated near the heater so that there would be little signal between 40 μs and $\sim$48 μs. We now understand that the expansion is much more subtle. A theoretical treatment[30] has shown that along the central axis of the pulse propagation, there is no cooling by expansion for approximately 5 mm from the heater. Hence in the model used here we only include cooling by *h*-phonon emission.

The model is essentially the same as that described in the following paper,[1] where it is developed analytically and a computer is only used to evaluate integrals. In our computer model, the *l*-phonon pulse is time-stepped through its propagation path and the *h*-phonons, emitted at each time step, are collected in time-labeled bins at the detector position, at times determined by the group velocities. The temperature of the *l*-phonon pulse is also calculated at each time step. Finally, the effect of the detector time constant is applied to give a simulation that can be directly compared with the measured signal. The key ingredients of the model are identical to those in Ref. 1. As in Ref. 4 Eq. (3), we start from the kinetic equation for the distribution function $n_{\rm h}$ for the *h*-phonons. For short pulses we ignore *h*-phonon decays in the *l*-phonon pulse, hence we get

$$\frac{dn_{\rm h}}{dt} = n_{\rm h}^{(0)}(p,T)\,\nu_{\rm b1}(p,T), \tag{4}$$

where $n_h^{(0)}$ is the Bose-Einstein distribution function,

$$n_{\rm h}^{(0)} = [\exp(\epsilon/kT) - 1]^{-1} \tag{5}$$

and $\nu_{\rm b1}$ is the creation rate by type 1, 4pp scattering.[5] In this section ϵ is in energy units for clarity. Multiplying both sides of Eq. (4) by $\Omega_{\rm p}\epsilon p^2 \delta p/(2\pi\hbar)^3$, where $\Omega_{\rm p}$ is the occupied solid angle in momentum space, we obtain

$$\frac{d}{dt}(\delta E_{\rm h}) = \delta E_{\rm h}^{(0)}(p,T)\,\nu_{\rm b1}(p,T), \tag{6}$$

where

$$\delta E_{\rm h} = \frac{\Omega_{\rm p}\epsilon p^2 n_{\rm h}\delta p}{(2\pi\hbar)^3}. \tag{7}$$

$\delta E_{\rm h}$ is the energy density of the *h*-phonons in the pulse in the momentum interval $p \to p + \delta p$, and

$$\delta E_{\rm h}^{(0)} = \frac{\Omega_p \epsilon p^2 n_{\rm h}^{(0)}\delta p}{(2\pi\hbar)^3}. \tag{8}$$

The creation rate is parametrized as,[1]

$$\nu_{\rm b1} = 1.228\times 10^9 \exp(-3.18\ [{\rm K}]/T) \times \exp(-1.65\ [{\rm K}^{-1}](p-p_{\rm c})c/k){\rm s}^{-1}, \tag{9}$$

where $p_{\rm c}c/k = 10$ K and the energy of the *h*-phonon is given by,[4]

$$\epsilon = 2.06\ [{\rm K}]{\rm k} + 0.794\ \ {\rm cp}. \tag{10}$$

From energy conservation we have,[4]

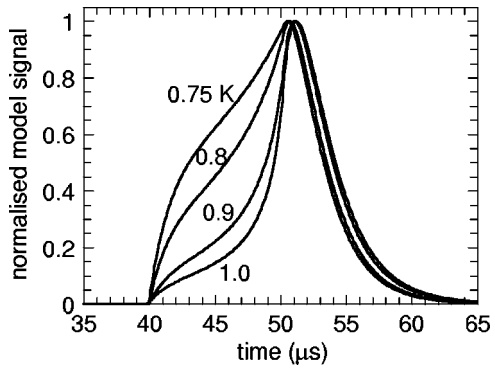

FIG. 10. The modeled *h*-phonon signal as a function of time after the heater pulse for different initial pulse temperatures 0.75 K, 0.8 K, 0.9 K, and 1 K, normalized to unity at the peak. Note the relative increase in the early arriving signal, 40–50.4 μs, as the initial temperature is decreased.

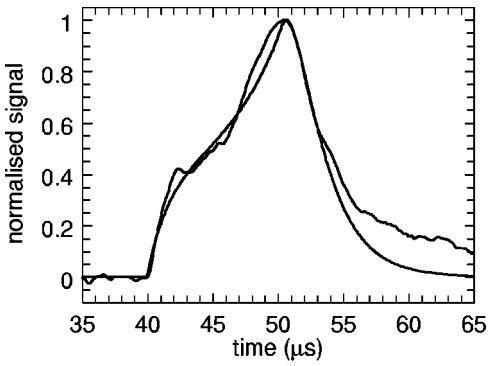

FIG. 11. The modeled signal with $T_i = 0.78$ K is compared to a short- and low-powered measured *h*-phonon signal 80 ns and 3.2 mW. The remanent *l*-phonon signal causes the small peak at 42 μs. The fit is satisfactory except at long times where the measured signal is much larger, which is probably due to an artifact.

$$\frac{dE_l}{dt} = -\frac{dE_h}{dt} \tag{11}$$

where E_h and E_l are the energy densities of the *h*- and *l*-phonons, respectively; E_h is found by integrating δE_h over momentum and E_l is given by Eq. (3).

Equations (11) and (3) allow the new value of T to be found after an increment of E_h has been lost from the *l*-phonon pulse. The new value of T is then used to calculate new values of ν_{b1} and $\delta E_h^{(0)}$ and hence the next increment E_h can be found from Eq. (5). This energy then propagates to the detector at the momentum dependent group velocity. The group velocity $v_g(p)$ is given by

$$v_g = 189\ [\mathrm{m\,s^{-1}}] - 18.5\ [\mathrm{m\,s^{-1}K^{-1}}](p - p_c)c/k. \tag{12}$$

The only free parameter is the starting temperature T_i of the *l*-phonon pulse. We take $\Omega_p = 0.115$ sr corresponding to $\theta_{3pp} = 11°$. The simulation gives similar results to those in Ref. 1, which gives us confidence in both results. In Fig. 10 we show the computer simulation signals for several initial temperatures, normalized to the same peak height. We see that the signal increases between 40 and 50.4 μs as T_i is lowered. This follows directly from the lower creation rate at lower temperatures, which lowers the rate of cooling of the pulse, so *h*-phonons are created over the whole propagation path, in particular near to the bolometer, which creates the fastest signals.

In Fig. 11 we show a comparison between a measured signal and the model with $T_i = 0.78$ K. We choose a signal from a short and low power pulse so that it conforms as close as is possible to the short-pulse assumption in the model. We selected 80 ns and 3.2 mW as this signal has a better signal to noise ratio than ones with shorter pulse lengths. We see that the general shapes agree. The measured signal does not drop as rapidly as the modeled signal at long times but this we think is an artifact due to the bolometer substrate.

VI. CONCLUSIONS

A short heat pulse injected into liquid ^{4}He creates a pulse of strongly interacting low-energy phonons. High-energy phonons are created by 4pp interactions within this pulse, but are the left behind the pulse due to their group velocities being lower than the velocity of the pulse. Usually a bolometer detects both the groups of phonons. The low-energy-phonon pulse creates a signal which has a decay time constant of ~ 1.5 μs due to the detection system. There is also a low-level response which we provisionally attribute to the energy slowly leaking out of the bolometer substrate, over tens of microseconds after the pulse has been absorbed. These time constants make it very different to separate the *l*- and *h*-phonon contributions to the signal. So it is very useful to have separately detected these contributions.

This paper reported conditions where the bolometer is not responsive to *l*-phonons, so the signal is essentially only due to the *h*-phonons. The condition is easy to achieve; the bolometer is turned away from being face-on to the phonon beam and then left. When the normal to the bolometer is at 40° to the phonon propagation direction then we estimate that *l*-phonon contribution is less than 1% at 3.5 μs after the start of the signal. Using this technique we have measured the *h*-phonons signal at various heater power and pulse lengths.

We find that the variation in the *h*-phonon signal is not as large as the model calculations, with different initial temperatures for the *l*-phonons, suggest. This leads us to our conjecture that the initial temperatures are limited to the range from ≈ 0.75 K to ≈ 0.9 K. If the temperature is < 0.75 K few *h*-phonons are created and if it is > 0.9 K then relatively too few *h*-phonons are created in the early part of the signal.

The model only applies to short pulses in which the *h*-phonons leave the *l*-phonon pulse without scattering. We find that there is an agreement between the measured signal from a low power and short pulse, and the model with an initial temperature of 0.78 K. For higher pulse powers, the initial temperature seems limited to around ~ 0.9 K and the increase in the total energy of the *h*-phonons is mainly due to

the occupied solid angle in momentum space, increasing with pulse power.

The integrated *h*-phonon signal is proportional to the energy in the *h*-phonon system. We find that this energy is a universal function of the heater pulse energy, for pulse lengths that are not too long, see Figs. 9(a) and 9(b). The relationship is linear at low pulse energies but then falls increasingly below linear at higher pulse energies. The linear behavior is expected if a constant fraction of the *l*-phonon energy is converted to *h*-phonons within the pulse, and if the *h*-phonons can escape the *l*-phonon pulse without scattering. The first condition would be attained if the initial temperature of the *l*-phonons were constant, which we believe occurs for powers greater than ~ 7 mW. The second condition occurs in short pulses. When this second condition is not met, the data follow a curve which peels away from the universal curve. The less than linear increase, at higher pulse energies, has yet to be explained in detail, but it is likely to involve the scattering of *h*-phonons both inside and outside of the *l*-phonon pulse.

The *h*-phonons with energy ~ 10 K are the main contributors to the signal between 40 μs and 50.4 μs. We have integrated the signal over this range and also over 40–60 μs. The ratio of these integrals is a measure of the contribution of the 10 K phonons to the total *h*-phonon energy. We find this ratio decreases rapidly with pulse power at low powers, see Fig. 7. This shows that the spectrum of *h*-phonons shifts to higher energies, and hence lower group velocities, as the pulse power is initially increased. In the low power range, the initial temperature of the *l*-phonon pulse increases with pulse power, but we see that this behavior ceases at higher powers. This is another indication that there is a limit to the initial *l*-phonon temperature that can be created, as higher energy *h*-phonons are more readily created at higher temperatures.

In the future we need to understand what causes the bolometer signal at long times >60 μs; is it simply due to absorbed energy in the bolometer substrate leaking out slowly? Theoretically we need to explain the shapes of the universal curves in Figs. 5 and 9, and explore the possible reasons why the initial temperature of the *l*-phonon pulse appears to have a maximum value and how the occupied solid angle in momentum space increases with the pulse power.

In summary, we have shown clearly that phonons are created throughout the 9.5 mm path between the heater and bolometer and that the *h*-phonon signal shape can be explained in some detail for short pulses, using a model which incorporates the theoretical creation rate as a function of *h*-phonon momentum and initial temperature. The success of this one-dimensional model, with no explicit lateral expansion of the *l*-phonon pulse, adds credibility to the recent theory of lateral expansion which shows that expansion has no effect on the temperature of the *l*-phonon pulse, along the central axis of propagation for 5 mm. From the behavior of the *h*-phonon pulse as a function of power, we have conjectured that there is a limit to the *l*-phonon temperature as the pulse power is raised and this must be resolved in the future.

ACKNOWLEDGMENTS

We would like to thank I. N. Adamenko for many helpful discussions, EPSRC for Grants Nos. GR/N20225 and GR/S24855/01 and S. Tuckett for constructing the apparatus.

[1] I.N. Adamenko, K.E. Nemchenko, V.A. Slipko, and A.F.G. Wyatt, following paper, Phys. Rev. B **69**, 144525 (2004).
[2] M.A.H. Tucker and A.F.G. Wyatt, J. Phys.: Condens. Matter **6**, 2813 (1994).
[3] I.N. Adamenko, K.E. Nemchenko, A.V. Zhukov, M.A.H. Tucker, and A.F.G. Wyatt, Phys. Rev. Lett. **82**, 1482 (1999).
[4] A.F.G. Wyatt, M.A.H. Tucker, I.N. Adamenko, K.E. Nemchenko, and A.V. Zhukov, Phys. Rev. B **62**, 9402 (2000).
[5] I.N. Adamenko, K.E. Nemchenko, and A.F.G. Wyatt, J. Low Temp. Phys. **126**, 1471 (2002).
[6] S. Havlin and M. Luban, Phys. Lett. **42A**, 133 (1972).
[7] M.A.H. Tucker, A.F.G. Wyatt, I.N. Adamenko, A.V. Zhukov, and K.E. Nemchenko, Fiz. Nizk. Temp. **25**, 657 (1999) [J. Low Temp. Phys. **25**, 488 (1999)].
[8] H.J. Maris and W.E. Massey, Phys. Rev. Lett. **25**, 220 (1970).
[9] J. Jäckle and K.W. Kerr, Phys. Rev. Lett. **27**, 654 (1971).
[10] W.G. Stirling, in *75th Jubilee Conference on Liquid Helium-4*, edited by J. G. M. Armitage (World Scientific, Singapore, 1983), p. 109.
[11] R.C. Dynes and V. Narayanamurti, Phys. Rev. Lett. **33**, 1195 (1974).
[12] A.F.G. Wyatt, N.A. Lockerbie, and R.A. Sherlock, Phys. Rev. Lett. **33**, 1425 (1974).
[13] I.M. Khalatnikov, *An Introduction to the Theory of Superfluidity* (Addison Wesley, Redwood City, California, 1989).
[14] S.G. Eckstein, Y. Eckstein, J.B. Ketterson, and J.H. Vignos, *Physical Acoustics* (Academic Press, New York, 1970), Vol. II, p. 244.
[15] M.A.H. Tucker and A.F.G. Wyatt, J. Phys.: Condens. Matter **4**, 7745 (1992).
[16] I.N. Adamenko, K.E. Nemchenko, A.V. Zhukov, M.A.H. Tucker, and A.F.G. Wyatt, Physica B **284-288**, 31 (2000).
[17] M.A.H. Tucker and A.F.G. Wyatt, J. Low Temp. Phys. **113**, 621 (1998).
[18] R.A. Sherlock and A.F.G. Wyatt, J. Phys. E **16**, 673 (1983).
[19] P.C. Hendry and P.V.E. McClintock, Cryogenics **27**, 131 (1987).
[20] See review by A.C. Anderson, in *Non Equilibrium Superconductivity, Phonons, and Kapitza Boundaries*, edited by K.E. Gray (Plenum Press, New York, 1981).
[21] G.J. Page and A.F.G. Wyatt, J. Phys. C **11**, 4927 (1978).
[22] R.A. Sherlock, N.G. Mills, and A.F.G. Wyatt, J. Phys. C **8**, 300 (1975).
[23] A.F.G. Wyatt and G.N. Crisp, J. Phys., Colloq. C6, Supp. 8, **39**, C6-244 (1978).
[24] L.J. Challis, J. Phys. C **7**, 481 (1974).
[25] T.W. Bradshaw and A.F.G. Wyatt, J. Phys. C **16**, 651 (1983).

[26] I.N. Adamenko, K.E. Nemchenko, and A.F.G. Wyatt, Fiz. Nizk. Temp. **28**, 123 (2002) [J. Low Temp. Phys. **28**, 85 (2002)].
[27] A.F.G. Wyatt, I.N. Adamenko, and K.E. Nemchenko, J. Low Temp. Phys. **126**, 609 (2002).
[28] I.N. Adamenko, K.E. Nemchenko, and A.F.G. Wyatt, Fiz. Nizk. Temp. **29**, 16 (2003) [J. Low Temp. Phys. **29**, 11 (2003)].
[29] R. Vovk, C.D.H. Williams, and A.F.G. Wyatt, Phys. Rev. B **68**, 134507 (2003).
[30] I.N. Adamenko, K.E. Nemchenko, V.A. Slipko, and A.F.G. Wyatt, Phys. Rev. B **68**, 134508 (2003).